

Exploiting Multipath Information for Integrated Localization and Sensing via PHD Filtering

Yinuo Du, Hanying Zhao, *Member, IEEE*, Yang Liu, Xinlei Yu, Yuan Shen, *Senior Member, IEEE*

Abstract—Accurate localization and perception are pivotal for enhancing the safety and reliability of vehicles. However, current localization methods suffer from reduced accuracy when the line-of-sight (LOS) path is obstructed, or a combination of reflections and scatterings is present. In this paper, we present an integrated localization and sensing method that delivers superior performance in complex environments while being computationally efficient. Our method uniformly leverages various types of multipath components (MPCs) through the lens of random finite sets (RFSs), encompassing reflections, scatterings, and their combinations. This advancement eliminates the need for the multipath identification step and streamlines the filtering process by removing the necessity for distinct filters for different multipath types, a requirement that was critical in previous research. The simulation results demonstrate the superior performance of our method in both robustness and effectiveness, particularly in complex environments where the LOS path is obscured and in situations involving clutter and missed detection of MPC measurements.

Index Terms—Integrated localization and sensing, multipath propagation environments, PHD filtering

I. INTRODUCTION

High-accuracy localization with environmental sensibility is a critical technology in autonomous driving and 6G communication systems [1]. However, achieving precise localization in complex propagation environments poses a significant challenge for vehicles, primarily due to obstructions, reflections, and signal scatterings, leading to interference and phase shifting of received signals. To bolster vehicle safety and reliability, it is essential to address these complexities in localization.

Conventional localization methods put great efforts into eliminating these effects to extract line-of-sight (LOS) signal for positioning. Nowadays, with the development of wireless technologies such as vehicle-mounted large bandwidth and large-scale antenna arrays, the high temporal- and spatial-resolution measurements enable us to separate mixed signals and estimate both the LOS signal and the non-line-of-sight (NLOS) multipath components (MPCs) [2]. Therefore, there are a growing number of localization methods that aim to exploit these multipath information to improve localization accuracy and achieve environmental sensing [3]–[6]. This topic is often referred to as radio simultaneous localization

Yinuo Du, Hanying Zhao and Yuan Shen are with the Department of Electronic Engineering, and Beijing National Research Center for Information Science and Technology, Tsinghua University, Beijing 100084, China (e-mail: duyn19@mails.tsinghua.edu.cn; {hying_zhao,shenyuan_ee}@tsinghua.edu.cn). Yang Liu and Xinlei Yu are with the Department of Standards Research, OPPO Inc., Beijing 100101, China (e-mail: liuyangbj@oppo.com; yuxinlei@oppo.com).

© 2024 IEEE. Personal use of this material is permitted. Permission from IEEE must be obtained for all other uses, in any current or future media, including reprinting/republishing this material for advertising or promotional purposes, creating new collective works, for resale or redistribution to servers or lists, or reuse of any copyrighted component of this work in other works.

DOI of the published paper is 10.1109/TVT.2024.3433028

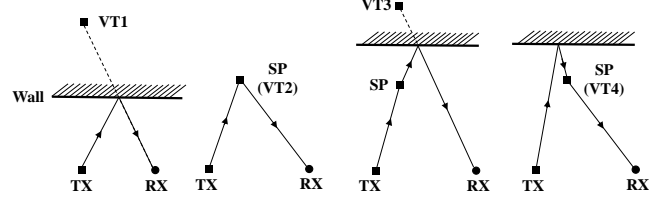


Fig. 1. An illustration to show the geometric relationships among transmitters (Tx), receivers (Rx), and VTs for various MPCs: planar reflections (left), scattering points (SP) (second from the left), and a combination of one scattering and one reflection (third and fourth from the left). The multipath signals can be perceived as if they were virtually emitted from VTs.

and mapping (SLAM). We give a brief review of them and make a comparison between existing works and ours.

In [3], the authors use a monostatic UWB device to detect and localize surrounding features. They adopt particle filtering with two methods of associating measurements with landmarks: Nearest Neighbor Data Association and Probabilistic Data Association. In [6], the authors use an adaptive federal filter to handle NLOS MPCs. However, their approach is limited to a specific number of MPCs and only considers reflection MPCs. Channel-SLAM in [4] treats multipath components as signals emitted from virtual transmitters (VTs), and an Rao-Blackwellised particle filter (RBPF) based on Recursive Bayesian filtering is employed to improve computational tractability by sampling particles in a subspace. Other works such as [7], [8] achieve radio SLAM using reconfigurable intelligent surfaces (RISs), where Murty’s algorithm is adopted to handle data association (DA) in [7]. As these works have mentioned, one of the main challenges of radio-SLAM lies in DA, i.e., assigning measurements to corresponding landmarks. In the domain of Bayesian SLAM, probability hypothesis density (PHD)-SLAM has garnered significant attention in recent years due to its superior performance compared to traditional RBPF-SLAM methods [9], [10]. Employing finite-set statistics (FISST), PHD-SLAM effectively addresses the complex DA problem by grouping time-varying elements into random finite sets (RFSs). This approach has been adopted in the context of radio-SLAM [11] in works such as [5] to tackle the DA issue. The authors in [5] proposed a cooperative vehicle positioning and radio environment mapping method via a multiple-model PHD filter. Although a promising performance is achieved, multiple PHD filters are derived and employed for different types of MPCs since MPCs originating from reflections and scatterings are treated distinctly. Moreover, this method fails to handle MPCs which are under the dual effect of scatterings and reflections.

In this paper, we present an integrated localization and sensing method that delivers superior performance in complex environments while being computationally efficient. Our method can uniformly leverage various types of MPCs, encom-

passing reflections, scatterings, and their combinations, thus bypassing the multipath identification step. The key enabler is the introduced MPC model represented as an RFS, which augments the state space to characterize the diverse geometric relationships between the agent and the environment for each MPC type. This advancement simplifies the filtering process by eliminating the requirement of separate filters for different types of MPCs, a step that was essential in previous studies like [5]. Our method offers more streamlined and versatile solutions for integrated localization and sensing in complex environments, which can serve as a practical guideline for implementation and advancement in areas such as autonomous driving and 6G.

II. SYSTEM MODEL

Consider a 2D localization scenario where a vehicle (agent) receives wireless signals transmitted from a static base station (anchor) for positioning.¹ Let $\mathbf{r}_b = [x_b \ y_b]^T$ denote the position of the stationary anchor. At time instant t_k with $k \in \mathbb{Z}^+$, the agent state can be described by

$$\mathbf{x}_k = [\mathbf{r}_k^T \ \mathbf{v}_k^T \ b_k]^T \quad (1)$$

where $\mathbf{r}_k = [x_k \ y_k]^T$, $\mathbf{v}_k = [v_{x_k} \ v_{y_k}]^T$ and b_k denote position, velocity and ranging bias incurred by clock offset, respectively. At time $t_{k+1} := t_k + \Delta t$, the agent new state yields:

$$\mathbf{x}_{k+1} = \mathbf{A}\mathbf{x}_k + \mathbf{B}\mathbf{n}_k \quad (2)$$

where $\mathbf{n}_k = [u_{x,k} \ u_{y,k} \ u_{b,k}]^T$ is the process noise modelled as additive white Gaussian noise (AWGN) with variances σ_x^2 , σ_y^2 and σ_b^2 . \mathbf{A} and \mathbf{B} are transition matrices, which can be obtained from $\mathbf{r}_{k+1} = \mathbf{r}_k + \mathbf{v}_k \Delta t + [u_{x,k} \ u_{y,k}]^T \Delta t^2 / 2$, $\mathbf{v}_{k+1} = \mathbf{v}_k + [u_{x,k} \ u_{y,k}]^T \Delta t$, and $b_{k+1} = b_k + u_{b,k} \Delta t$.

A. Multipath Model

In complicated environments, where reflection surfaces (like exterior walls of buildings) and scatterers (like smaller objects along the road) are common, wireless signals often reflect and scatter before reaching the agent via multiple paths. As NLOS MPCs embed information pertinent to both agent localization and environmental context, we exploit those MPCs to enhance localization accuracy and achieve environment sensing.

In general, NLOS MPCs can be categorized into three types, as shown in Fig. 1: 1) MPCs induced by reflections; 2) MPCs caused by scatterings; and 3) MPCs influenced by both scatterings and reflections. The diverse geometric relationships between the agent and the environment for each MPC type present a significant challenge: identifying these heterogeneous multipaths. This involves determining the specific category to which each MPC belongs. To overcome this deficiency, we introduce a special form of virtual transmitters (VTs), allowing us to treat all types of MPCs in a unified way.

¹Our method is also applicable to 3D scenarios and multi-anchor systems. In 3D scenarios, it is adapted by adding elevation angles to the observation space and incorporating the z -axis into the state space. For multi-anchor systems, our approach is extended by augmenting observations from all anchors within the observation space.

Through the lens of VT, all NLOS MPCs can be modeled as if they are virtually emitted from VTs [4] and described as

$$\mathbf{m}^{(l)} = \left[(\mathbf{r}_{vt}^{(l)})^T \ b_{vt}^{(l)} \right]^T \quad (3)$$

where $\mathbf{r}_{vt}^{(l)} = [x_{vt}^{(l)} \ y_{vt}^{(l)}]^T \in \mathbb{R}^2$ denote the 2-D position of the l -th VT and $b_{vt}^{(l)}$ is the additional propagation length of this MPC. Taking the four MPCs in Fig. 1 for illustration:

- 1) The reflection MPC can be viewed as being directly transmitted from the VT which is the anchor's mirror image to the reflector (VT1);
- 2) The MPC induced by a scatterer can be viewed as being directly transmitted from the scatterer $\mathbf{r}_{vt}^{(2)} := \mathbf{r}_S = [x_S \ y_S]^T$ with an additional propagation bias $b_{vt}^{(2)} = \|\mathbf{r}_b - \mathbf{r}_S\|_2$ (VT2);
- 3) The MPCs under the dual effect of scattering and reflection can also be viewed as being directly transmitted from a VT with an additional propagation bias. As in Fig. 1, MPCs of VT3 and VT4 are composed of one reflection and one scattering each, albeit in a different sequence. VT3 is located at the scatterer's mirror image to the reflector with $b_{vt}^{(3)} = \|\mathbf{r}_b - \mathbf{r}_S\|_2$ and VT4 is located at the same location as the scatterer with $b_{vt}^{(4)} = \|\mathbf{r}_b - \mathbf{r}_{vt}^{(3)}\|_2$.

B. Formulating Multipath Components Using RFS

As MPCs emerge and die along with the movement of the agent, and due to clutter and the missed detection phenomena, we need to identify which VTs are present and more importantly, manage the NP-hard DA task for both VTs and observations across various time instances. To address this issue, we group VTs and wireless measurements into RFSs [12] instead of the conventional matrices. By adopting the RFS framework, we can more adeptly characterize the stochastic nature of both the detection process and the environment's dynamics for radio-SLAM. We formulate the VT map, which encompasses all detected VTs, as an RFS to accommodate its time-varying characteristics. This set at time instant t_k is denoted by $\mathcal{M}_k = \{\mathbf{m}_k^{(1)}, \mathbf{m}_k^{(2)}, \dots, \mathbf{m}_k^{(|\mathcal{M}_k|)}\}$.

Remark 1: The benefits of this VT model are summarized as follows: First, our method enables a consistent description and utilization of all types of MPCs, including those arising from multiple reflections and scatterings. In contrast, other approaches use distinct models for different types of MPCs, necessitating the identification of the MPC type prior to filtering or the usage of multiple filters in the filtering stage. Moreover, existing methods are unable to tackle MPCs affected by the combined effects of reflections and scatterings. Second, a challenge encountered in previous works is the difficulty to distinguish MPCs whose VTs are located at the same spatial position. This situation often arises when different MPCs undergo the same scatterer before reaching the receiver, such as VT2 and VT4 in Fig. 1. The introduced VT model overcomes this challenge by including the additional propagation bias parameter, as shown in (3), which is distinct for VT2 and VT4, allowing for their differentiation. This feature facilitates the development of the method for accurately discerning environmental characteristics. Third, utilizing RFSs, we explicitly bypass the NP-hard DA step. These advantages

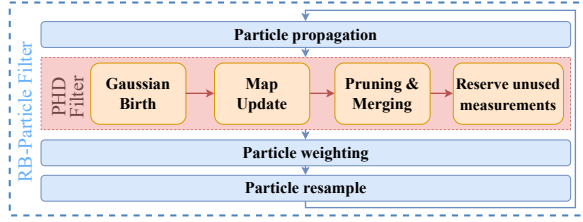


Fig. 2. A General Look at the complete PHD-SLAM algorithm

highlight the effectiveness and practicality of our VT model in handling complex propagation environments and leveraging multipath information for improved localization and sensing.

On the other hand, the time-of-arrivals (ToAs) and angle-of-arrivals (AoAs) of detected MPCs are estimated from the channel impulse response (CIR) [6] [13]. Then, the entire set of measurements at time instant t_k under the RFS framework can be described by

$$\mathcal{Z}_k = \{\mathcal{Z}_k^{(0)}, \mathcal{Z}_k^{\text{NLOS}}\} \quad (4)$$

where RFSs $\mathcal{Z}_k^{(0)}$ and $\mathcal{Z}_k^{\text{NLOS}}$ describe the LOS and the NLOS measurements at time instant t_k , respectively, which are non-empty when LOS signal/NLOS MPCs are detected or false alarms occur, and are empty otherwise, i.e.

$$\mathcal{Z}_k^{(0)} = \begin{cases} \{\mathbf{z}_k^{(0)}\}, & \text{LOS signal detected,} \\ \emptyset, & \text{LOS signal miss,} \end{cases} \quad \mathcal{Z}_k^{\text{NLOS}} = \bigcup_{l \geq 1} \{\mathbf{z}_k^{(l)}\}$$

and the detection probability for a VT located at \mathbf{m} with the agent located at \mathbf{x} is denoted as $P_D(\mathbf{m}, \mathbf{x})$. The range-bearing observation of the l -th VT $\mathbf{m}_k^{(l)}$ is

$$\mathbf{z}_k^{(l)} = \begin{bmatrix} \mathbf{d}_k^{(l)} \\ \boldsymbol{\theta}_k^{(l)} \end{bmatrix} = \begin{bmatrix} \|\mathbf{r}_k - \mathbf{r}_{\text{vt}}^{(l)}\|_2 + \mathbf{b}_k + \mathbf{b}_{\text{vt}}^{(l)} \\ \arctan\left(\frac{y_{\text{vt}}^{(l)} - y_k}{x_{\text{vt}}^{(l)} - x_k}\right) \end{bmatrix} + \boldsymbol{\omega}_k^{(l)} \quad (5)$$

in which $\boldsymbol{\omega}_k^{(l)}$ denotes the AWGN with standard deviation σ_d and σ_θ for the range and the bearing measurements, respectively. The LOS measurement $\mathbf{z}_k^{(0)}$ has the same structure as that in (5) but with noise standard deviations $\sigma_d^{(0)}$ and $\sigma_\theta^{(0)}$. All the measurements at time instance t_k , including real measurements and clutter are grouped in (4).

To achieve integrated localization and sensing, we aim to simultaneously estimate the agent trajectory $\mathbf{x}_{0:k}$ and the VT map \mathcal{M}_k based on $\mathcal{Z}_{1:k}$, representing measurements from t_1 to t_k , i.e., computing the posterior distribution $p(\mathbf{x}_{0:k}, \mathcal{M}_k | \mathcal{Z}_{1:k})$.

Remark 2: A potential limitation of our VT model is its requirement for multi-shot measurements. This is because the VT's state is characterized by a 3-D vector, whereas the range-bearing measurements at a one time stamp are 2-D. To let the volume of observations surpass the number of unknowns, we leverage multi-shot measurements and determine the agent trajectory alongside the states of VTs through filtering.

III. INTEGRATED LOCALIZATION AND ENVIRONMENT SENSING VIA PHD FILTERING

Our method for estimating the agent trajectory and VT map includes four steps: particle propagation, map prediction, map update and particle reweight/resampling, as shown in Fig. 2.

The computation of $p(\mathbf{x}_{0:k}, \mathcal{M}_k | \mathcal{Z}_{1:k})$ using a homogeneous filter is challenging because \mathbf{x}_k is a vector and \mathcal{M}_k is an RFS. To address this problem, we decompose the posterior density based on the Rao-Blackwellisation step [14] in RBPFs

$$p(\mathbf{x}_{0:k}, \mathcal{M}_k | \mathcal{Z}_{1:k}) = p(\mathbf{x}_{0:k} | \mathcal{Z}_{1:k}) p(\mathcal{M}_k | \mathcal{Z}_{1:k}, \mathbf{x}_{0:k}) \quad (6)$$

where the first term on the right-hand side (RHS) is the marginal posterior probability distribution of the agent trajectory $\mathbf{x}_{0:k}$, and the second term is the conditional probability distribution of the VT map \mathcal{M}_k . Leveraging this decomposition, similar to the approach in [9], we construct an RBPF [14]. For a standard RBPF, the marginal distribution $p(\mathbf{x}_{0:k} | \mathcal{Z}_{1:k})$ is sampled using particles. For each particle, the conditional map $p(\mathcal{M}_k | \mathcal{Z}_{1:k}, \mathbf{x}_{0:k})$ should be iterated analytically [14]. Calculating and iterating the precise probability distribution of an RFS is computational intractable, thus we use a Poisson point process (PPP) to approximate the RFS by aligning its intensity function with the first-order statistical moment of the RFS, known as the probability hypothesis density (PHD). This approach forms a PHD filter [9], [10], details on the PHD of an RFS and the PHD filter can be found in [12].

A. Importance Sampling and Particle Propagation

At time instant t_k , N particles are used to describe the agent trajectory $\mathbf{x}_{0:k}$, where the posterior weight of the i -th particle with trajectory $\mathbf{x}_{0:k}^{(i)}$ is denoted as $w_{k|k}^{(i)}$. For the i -th particle, we use $v_{k|k}^{(i)}(\mathbf{m})$ to describe the PHD of the posterior VT map RFS $\mathcal{M}_k | \mathcal{Z}_{1:k}, \mathbf{x}_{0:k}^{(i)}$ at \mathbf{m} . Therefore, the posterior particle set at time instant t_k is:

$$\mathcal{P}_k = \{\mathbf{x}_{0:k}^{(i)}, v_{k|k}^{(i)}(\mathbf{m}), w_{k|k}^{(i)}\}_{i=1}^N. \quad (7)$$

The posterior probability density function (PDF) of the agent trajectory is approximated as: $p(\mathbf{x}_{0:k} | \mathcal{Z}_{1:k}) = \sum_{i=1}^N w_{k|k}^{(i)} \delta(\mathbf{x}_{0:k} - \mathbf{x}_{0:k}^{(i)})$. The conditional map distribution can be analytically approximated by its PHD as follows [12]:

$$p(\mathcal{M}_k | \mathcal{Z}_{1:k}, \mathbf{x}_{0:k}^{(i)}) = e^{-\int v_{k|k}^{(i)}(\mathbf{s}) d\mathbf{s}} \prod_{\mathbf{m}_k^{(l)} \in \mathcal{M}_k} v_{k|k}^{(i)}(\mathbf{m}_k^{(l)}). \quad (8)$$

In the particle propagation step at t_k , we estimate the predicted distribution $p(\mathbf{x}_{0:k} | \mathcal{Z}_{1:k-1})$ using \mathcal{P}_{k-1} . Particle trajectory $\mathbf{x}_{0:k}^{(i)}$ and the weight $w_{k|k-1}^{(i)}$ are predicted based on the principle of importance sampling [15]. We use the importance density $q(\mathbf{x}_{0:k}^{(i)} | \mathcal{Z}_{1:k})$ to sample particle states, which satisfies $q(\mathbf{x}_{0:k}^{(i)} | \mathcal{Z}_{1:k}) = q(\mathbf{x}_k^{(i)} | \mathbf{x}_{0:k-1}^{(i)}, \mathcal{Z}_{1:k}) q(\mathbf{x}_{0:k-1}^{(i)} | \mathcal{Z}_{1:k-1})$ and calculate predicted particle weight $w_{k|k-1}^{(i)}$ by

$$w_{k|k-1}^{(i)} \propto w_{k-1|k-1}^{(i)} \frac{p(\mathbf{x}_k^{(i)} | \mathbf{x}_{k-1}^{(i)})}{q(\mathbf{x}_k^{(i)} | \mathbf{x}_{0:k-1}^{(i)}, \mathcal{Z}_{1:k})}. \quad (9)$$

Similar to the widely adopted approach in [5], [9], [10], we use the motion model to characterise the importance density. Specifically, we use $q(\mathbf{x}_k^{(i)} | \mathbf{x}_{0:k-1}^{(i)}, \mathcal{Z}_{1:k}) = p(\mathbf{x}_k^{(i)} | \mathbf{x}_{k-1}^{(i)})$ to simplify calculations, which yields $w_{k|k-1}^{(i)} = w_{k-1|k-1}^{(i)}$.

B. PHD Filtering

Next, we address each particle's VT map individually. For the posterior PHD of the VT map for the i -th particle at time

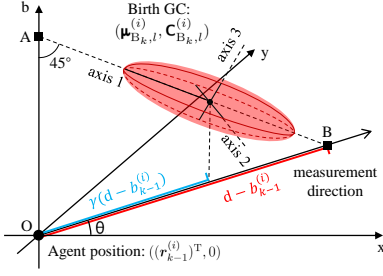


Fig. 3. For the i -th particle with state $\mathbf{x}_k^{(i)}$ at time instant t_k , parameters of the birth GC ($\boldsymbol{\mu}_{B_{k,l}}^{(i)}, \mathbf{C}_{B_{k,l}}^{(i)}$) is generated according to the measurement $\mathbf{z}_{B_{k,l}} = [d, \theta]^T$ and the particle state $\mathbf{x}_{k-1}^{(i)}$. $\boldsymbol{\mu}_{B_{k,l}}^{(i)}$ is constrained on the line AB. axis 1,2,3 are the three main axes of the GC's confidence ellipsoid, where axis 1 is set along line AB and axis 3 is set within plane OAB.

t_k , we model it using a Gaussian-mixture (GM) form [9]:

$$v_{k|k}^{(i)}(\mathbf{m}) = \sum_{j=1}^{M_{k|k}^{(i)}} \alpha_{k|k,j}^{(i)} \mathcal{N}(\mathbf{m}; \boldsymbol{\mu}_{k|k,j}^{(i)}, \mathbf{C}_{k|k,j}^{(i)}) \quad (10)$$

where $M_{k|k}^{(i)}$ is the number of Gaussian components (GCs) in the GM. After the particle propagation at time stamp t_k , only $v_{k-1|k-1}^{(i)}(\mathbf{m})$ is accessible. To compute $v_{k|k}^{(i)}(\mathbf{m})$, we iterate through two steps: prediction and update.

1) *PHD Prediction*: In complex propagation environments, MPCs emerge and die along with the movement of the agent. To effectively process changeable VTs, we adopt the ‘‘adaptive birth strategy’’ [16], where the mean and variance of birth GCs are determined by measurements, rather than using a fixed birth GC distribution. This strategy has been widely employed in Gaussian-mixture (GM)-PHD filters and PHD-SLAM works, such as [5], [10]. Here, to generate a 3-D GC based on 2-D range-bear measurements at a single stamp, we derive a new method to generate birth GCs, which is tailored specifically for our VT model.

As shown in Fig. 3, for particle i , suppose there are $B_k^{(i)}$ MPC measurements that do not match with any existing VTs at time instant t_{k-1} . To simplify the notations, suppose that the l -th unmatched MPC measurement has the value of $\mathbf{z}_{B_{k,l}} = [d, \theta]^T$, we generate a birth GC with respect to this measurement, taking the form:

$$v_{B_{k,l}}^{(i)}(\mathbf{m}) = \mathcal{N}(\mathbf{m}; \boldsymbol{\mu}_{B_{k,l}}^{(i)}, \mathbf{C}_{B_{k,l}}^{(i)})$$

and initialize the mean $\boldsymbol{\mu}_{B_{k,l}}^{(i)} = [(\mathbf{r}_{B_{k,l}}^{(i)})^T \mathbf{b}_{B_{k,l}}^{(i)}]^T$ and covariance $\mathbf{C}_{B_{k,l}}^{(i)}$ by the measurement \mathbf{z} as follows:

First, in case of the birth GC's mean $\boldsymbol{\mu}_{B_{k,l}}^{(i)}$, with angle measurement θ , we set $\mathbf{r}_{B_{k,l}}^{(i)}$ to the same direction relative to the agent state as θ . With range measurement d , we have:

$$\|\mathbf{r}_{k-1}^{(i)} - \mathbf{r}_{B_{k,l}}^{(i)}\|_2 + b_{B_{k,l}}^{(i)} + b_{k-1}^{(i)} = d \quad (11)$$

due to the unknown additional propagation bias $\mathbf{b}_{B_{k,l}}^{(i)}$, $\mathbf{r}_{B_{k,l}}^{(i)}$ still has ambiguity, to address this issue, we introduce parameter γ ($0 \leq \gamma \leq 1$), where

$$\|\mathbf{r}_{k-1}^{(i)} - \mathbf{r}_{B_{k,l}}^{(i)}\|_2 = \gamma(d - b_{k-1}^{(i)}) \quad (12)$$

which allows us to control the mean of birth GC by γ .

Second, in case of the GC's covariance $\mathbf{C}_{B_{k,l}}^{(i)}$, we set:

$$\mathbf{C}_{B_{k,l}}^{(i)} = \mathbf{T}(\theta) \boldsymbol{\Sigma}(d) \mathbf{T}(\theta)^T \quad (13)$$

where $\mathbf{T}(\theta)$ is a three-dimension rotational matrix, given by

$$\mathbf{T}(\theta) = \begin{bmatrix} \frac{\cos(\theta)}{\sqrt{2}} & -\sin(\theta) & \frac{\cos(\theta)}{\sqrt{2}} \\ \frac{\sin(\theta)}{\sqrt{2}} & \cos(\theta) & \frac{\sin(\theta)}{\sqrt{2}} \\ -\frac{1}{\sqrt{2}} & 0 & \frac{1}{\sqrt{2}} \end{bmatrix} \quad (14)$$

and $\boldsymbol{\Sigma}(d)$ is a diagonal matrix depended on distance d by $[\boldsymbol{\Sigma}(d)]_{11} = \zeta \cdot (d - b_{k-1}^{(i)})^2$, $[\boldsymbol{\Sigma}(d)]_{22} = \iota \cdot (d - b_{k-1}^{(i)})^2 (\sigma_\theta)^2$ and $[\boldsymbol{\Sigma}(d)]_{33} = \xi \cdot (\sigma_d)^2$ with user-defined non-negative parameters ζ , ι , and ξ . $[\boldsymbol{\Sigma}(d)]_{11}$, $[\boldsymbol{\Sigma}(d)]_{22}$, $[\boldsymbol{\Sigma}(d)]_{33}$ denote the variance of the birth GC along axis 1,2 and 3 in Fig. 3 respectively.

Then, we predict the map PHD based on the summation of GMs [9] using the posterior map PHD at t_{k-1} and birth GCs as follows:

$$\begin{aligned} v_{k|k-1}^{(i)}(\mathbf{m}) &= v_{k-1|k-1}^{(i)}(\mathbf{m}) + \sum_{l=1}^{B_k^{(i)}} \alpha_{B_{k,l}} \mathcal{N}(\mathbf{m}; \boldsymbol{\mu}_{B_{k,l}}^{(i)}, \mathbf{C}_{B_{k,l}}^{(i)}) \\ &= \sum_{j=1}^{M_{k|k-1}^{(i)}} \alpha_{k|k-1,j}^{(i)} \mathcal{N}(\mathbf{m}; \boldsymbol{\mu}_{k|k-1,j}^{(i)}, \mathbf{C}_{k|k-1,j}^{(i)}) \quad (15) \end{aligned}$$

where $M_{k|k-1}^{(i)} = M_{k-1|k-1}^{(i)} + B_k^{(i)}$ and $\alpha_{B_{k,l}}$ denotes the GC's birth weight.

2) *PHD Update*: With wireless measurements at time t_k , we then update the PHD map of each particle. For particle i , denoting $P_D(\boldsymbol{\mu}_{k|k-1,j}^{(i)}, \mathbf{x}_k^{(i)})$ as $P_{D,k,j}^{(i)}$, the posterior PHD is updated using the GM-PHD filter's corrector equation [17, Sec. 6.D]:

$$\begin{aligned} v_{k|k}^{(i)}(\mathbf{m}) &= \sum_{l=1}^{|\mathcal{Z}_k^{\text{NLOS}}|} \sum_{j=1}^{M_{k|k-1}^{(i)}} \alpha_{k,l,j}^{(i)} \mathcal{N}(\mathbf{m}; \boldsymbol{\mu}_{k,l,j}^{(i)}, \mathbf{C}_{k,l,j}^{(i)}) \\ &+ \sum_{j=1}^{M_{k|k-1}^{(i)}} (1 - P_{D,k,j}^{(i)}) \alpha_{k|k-1,j}^{(i)} \mathcal{N}(\mathbf{m}; \boldsymbol{\mu}_{k|k-1,j}^{(i)}, \mathbf{C}_{k|k-1,j}^{(i)}) \end{aligned} \quad (16)$$

where the second term is induced by missed detections. For the first term, $\boldsymbol{\mu}_{k,l,j}^{(i)}$ and $\mathbf{C}_{k,l,j}^{(i)}$ are the mean and variance of the j -th GC corrected by the l -th measurement in $\mathcal{Z}_k^{\text{NLOS}}$ using extended Kalman filters (EKFs) [9]. Moreover, we model clutter as a Poisson point process with intensity $\kappa(\mathbf{z})$ and the expected number of clutter as λ_c . The corrected GCs' weights can be updated like a common PHD filter as in [9], [10]:

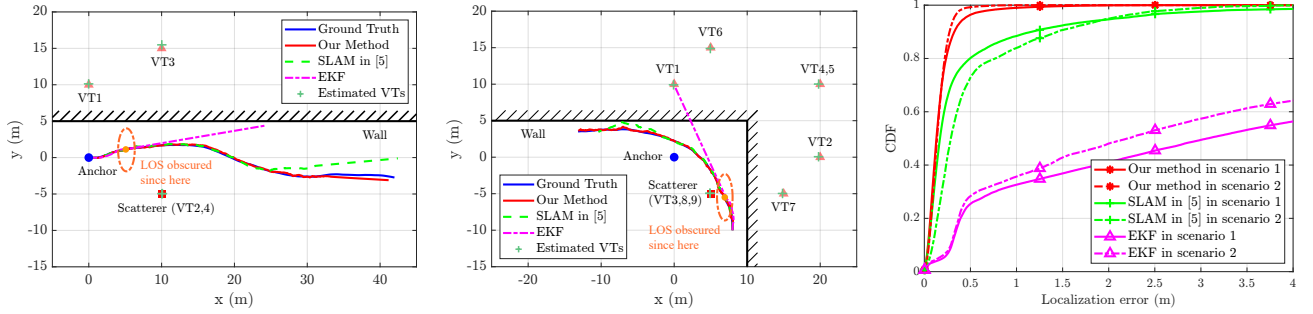
$$\alpha_{k,l,j}^{(i)} = \frac{P_{D,k,j}^{(i)} \alpha_{k|k-1,j}^{(i)} q_{k,j}^{(i)}(\mathbf{z}_k^{(l)})}{\kappa(\mathbf{z}_k^{(l)}) + \sum_{s=1}^{M_{k|k-1}^{(i)}} P_{D,k,s}^{(i)} \alpha_{k|k-1,s}^{(i)} q_{k,s}^{(i)}(\mathbf{z}_k^{(l)})} \quad (17)$$

where $q_{k,j}^{(i)}(\mathbf{z}_k^{(l)})$ is the probability density of the l -th measurement raised by the j -th VT GC [9]. In the filtering process, coarse gating [17] is employed to ease computational burden and determine which MPC measurements are reserved for prediction in the next time stamp.

C. Particle Reweight and Resample

Combing the updated VT map and agent state, we have:

$$\begin{aligned} p(\mathbf{x}_{0:k} | \mathcal{Z}_{1:k}) &\propto p(\mathbf{x}_{0:k}, \mathcal{Z}_k | \mathcal{Z}_{1:k-1}) \\ &= p(\mathcal{Z}_k | \mathbf{x}_{0:k}, \mathcal{Z}_{1:k-1}) p(\mathbf{x}_{0:k} | \mathcal{Z}_{1:k-1}). \end{aligned} \quad (18)$$



(a) Scenario 1: VT1 with 1 reflection, VT2 with 1 scattering, VT3 and VT4 with 1 reflection and 1 scattering. (b) Scenario 2: VT1, VT2 with 1 reflection, VT3 with 1 scattering, VT4, VT5 with 2 reflections, VT6,7,8,9 with 1 reflection and 1 scattering. (c) The CDF of localization errors of three methods in two scenarios.

Fig. 4. (a) and (b) illustrate the configurations of 2 simulation scenarios and the localization results of one representative experiment of three methods for each scenario, (c) shows the CDF of localization errors.

The updated particle weight for particle i is thus given by

$$\begin{aligned} w_{k|k}^{(i)} &\propto p(\mathcal{Z}_k | \mathbf{x}_{0:k}^{(i)}, \mathcal{Z}_{1:k-1}) w_{k|k-1}^{(i)} \\ &= p(\mathcal{Z}_k^{(0)} | \mathbf{x}_k^{(i)}) p(\mathcal{Z}_k^{\text{NLOS}} | \mathbf{x}_{0:k}^{(i)}, \mathcal{Z}_{1:k-1}) w_{k|k-1}^{(i)} \end{aligned} \quad (19)$$

where the first term is the contribution of LOS measurement and is set equal for all particles if LOS measurement is lost. As shown in [10], the second term comes from the NLOS MPCs and satisfies

$$\begin{aligned} p(\mathcal{Z}_k^{\text{NLOS}} | \mathbf{x}_{0:k}^{(i)}, \mathcal{Z}_{1:k-1}) &= \\ p(\mathcal{Z}_k^{\text{NLOS}} | \mathbf{x}_{0:k}^{(i)}, \Lambda_k) \frac{p(\Lambda_k | \mathbf{x}_{0:k}^{(i)}, \mathcal{Z}_{1:k-1})}{p(\Lambda_k | \mathbf{x}_{0:k}^{(i)}, \mathcal{Z}_{1:k})} \end{aligned} \quad (20)$$

where Λ_k is a free map variable. Multiple strategies exist considering the choice of Λ_k , including empty-set strategy, single-feature strategy and multi-feature strategy [10]. To generate more accurate estimates, we adopt the multi-feature strategy to decide Λ_k , as shown in [10]. When the number of effective particles is low, particle resampling will be executed.

Finally, the agent trajectory is estimated based on the minimum-mean-square-error (MMSE) criteria using a weighted mean approach, and the VT map is estimated by extracting GCs with highest weights as demonstrated in previous works such as [9], [10].

IV. NUMERICAL RESULTS

In this section, two distinct simulation scenarios are investigated, with the layouts of their respective environments illustrated in Fig. 4(a) and Fig. 4(b). In the first scenario, shown in 4(a), there are a base station, a point scatterer, and a planar wall, located at $(0,0)\text{m}$, $(10,-5)\text{m}$, and along $y = 10\text{m}$, respectively. This configuration will lead to four NLOS MPCs and four corresponding VTs.² The second scenario, depicted in Fig. 4(b), presents a more complex propagation environment. It includes a base station located at $(0,0)\text{m}$, a point scatterer at $(5,-5)\text{m}$, a horizontal wall along $y = 5\text{m}$, and a vertical wall along $x = 10\text{m}$. This setup will result in 9 VTs. We also investigate the agent's field of view (FoV), which contributes

²While our method can handle MPCs with any combination of reflections and scatterings, in our simulations, we only consider NLOS MPCs related with either up to two reflections, two scatterings, or a combination of one reflection and one scattering.

to a more realistic representation of the real-life scenario. VTs located beyond the agent's FoV distance are not detected, aligning with practical limitations.

In both simulation scenarios, the simulation time is set to 30 seconds with measurement frequency at 12.5Hz. To assess validity in challenging propagation environments, the LOS measurements only exist in the first 6 seconds. We generate ground truth trajectories using the motion model in (2), with motion parameters $\sigma_x = \sigma_y = 0.5\text{m/s}^2$. Each trajectory undergoes 10 repetitions, during which distinct MPC measurements are generated using the measurement model in Section II-B for each repetition. Measurement noise parameters are set to $\sigma_d = 0.3\text{m}$, $\sigma_\theta = 4\text{deg}$ and $\sigma_d^{(0)} = 0.05\text{m}$, $\sigma_\theta^{(0)} = 2\text{deg}$, with $P_{D,k,j}^{(i)} = 0.95$ within a fixed-range FoV for the agent and $\lambda_c = 0.02$. For the filter setup, we set the particle number to $N = 1000$. The filter parameters associated with the measurement model and motion model, including the particles' initial states, align with those employed in the data generation step, and we set the noise parameter for the clock bias as $\sigma_b = 0.01\text{m/s}$. For birth GCs' parameters we discussed in (12) and (13) in Section III-B1, we set $\gamma = 0.7$, $\zeta = 0.1$, $\iota = 0.5$, $\xi = 0.3$ and $\alpha_B = 0.01$. Specifically, in the first scenario, utilizing 10 trajectories and 100 simulations, the agent initial position and velocity are $(0,0)\text{m}$ and $(1,0)\text{m/s}$ respectively with $b_0 = 0.3\text{m}$. In particular, the agent's FoV is 35m. In the second scenario, which encompasses 5 trajectories and 50 simulations, the initial state and velocity for the agent are designated as $(8,-10)\text{m}$ and $(0,1)\text{m/s}$, respectively, with $b_0 = 0.3\text{m}$, and the FoV is set to 25m.

To evaluate the effectiveness of our method, we compare it with the approach presented in [5], where two different PHD filters are used for handling the reflection and scattering MPCs separately. We also compare our method with an EKF-based method that only utilizes LOS measurements as a performance baseline. The parameters in these methods align with those employed in the data generation step. The estimated trajectories from one experiment are visualized in Fig. 4(a) and Fig. 4(b). The CDF of the localization error across all simulation runs is shown in Fig. 4(c), and the root mean squared errors (RMSEs) of the 2-D position estimates for all VTs are shown in Tables I and II. The time complexity of our method and the SLAM in [5] per iteration are both in

TABLE I
THE RMSES OF VT ESTIMATES IN SCENARIO 1

Method	VT1	VT2	VT3	VT4
Ours	0.40 m	0.39 m	0.66 m	0.46 m
SLAM in [5]	1.77 m	6.28 m	5.11 m	6.28 m

the order of $\mathcal{O}(N_k \times |\mathcal{M}_k| \times |\mathcal{Z}_k^{\text{NLOS}}|)$. For scenarios 1 and 2, respectively, the average computation time per iteration for our method is 17.6s and 29.2s, compared to 32.2s and 48.9s for the method in [5].³

Fig. 4 demonstrate the enhanced localization accuracy achieved by our method in both scenarios. In the first scenario, our method achieves a localization accuracy with an RMSE of 0.25m, which is 74.1% better than the SLAM approach in [5] with an RMSE=0.98m. It also outperforms the EKF baseline, which has an RMSE of 7.80m, by 96.8%. Similarly, in the second scenario, our method's RMSE of 0.18m surpasses that of the SLAM in [5] (RMSE 0.83m) by 78.1% and exceeds the EKF baseline (RMSE 7.83m) by 97.7%. Compared with other methods, Fig. 4 also shows the robustness of our method in scenarios where LOS is obscured, further demonstrating the robustness and superiority of our method in complex multipath scenarios with a limited FoV.

In terms of environmental sensing, our method excels in achieving sub-meter estimation accuracy in both scenarios, as demonstrated in Table I and II. In contrast, the radio-SLAM method in [5] cannot handle VTs influenced by both reflections and scatterings. As a result, it yields less accurate estimates for VT3,4 in scenario 1, and for VT6,7,8,9 in scenario 2.⁴

Remark 3: The method in [5] employs a closed-form strategy for importance weighting, while our approach utilizes a multi-feature strategy, as shown in (20). To conduct a brief ablation study, we test the same closed-form strategy from [5, Sec. 4.C] within our method. The resulting localization RMSEs for our method are 0.52m and 0.48m for scenarios 1 and 2, respectively. This represents a reduction in localization RMSE of 46.7% and 42.2% compared to the method in [5] for scenarios 1 and 2.

V. CONCLUSIONS

In this paper, we delivered high-accuracy localization and environmental sensing in an efficient and robust manner. The key to our method is the unified characterization and utilization of different types of MPCs via an RFS, which enables us to forge the requirement of identifying MPC types prior to filtering and eliminates the necessity for employing multiple MPC tracking filters. Moreover, our method also can handle MPCs influenced by both reflections and scatterings. The simulation results demonstrated that our method excels in

³The simulations are conducted using MATLAB, running on an Intel Xeon E5-2697 v4 @ 2.30GHz, under the Linux CentOS Stream 8 operating system.

⁴In Table I, VT2 and VT4 share the same 2-D position, since the method in [5] considers only the 2-D positions of VTs, it achieves identical RMSEs for two VTs. In Table II, VT8 and VT9 have identical RMSEs, while VT3 exhibits a different RMSE for the method in [5]. The reasons are as follows. Firstly, VT8 and VT9 share the same positions and propagation biases. Thus, in the GM-PHD map, VT8 and VT9 are often represented by a single GC with a weight close to 2. On the contrary, the GC corresponding to VT3 has a weight close to 1, separating it from VT8 and VT9.

TABLE II
THE RMSES OF VT ESTIMATES IN SCENARIO 2

Method	VT1	VT2	VT3	VT4,5
Ours	0.82 m	0.92 m	0.15 m	0.97 m
SLAM in [5]	1.68 m	1.45 m	0.98 m	1.55 m

Method	VT6	VT7	VT8,9
Ours	1.39 m	0.29 m	0.19 m
SLAM in [5]	4.54 m	4.52 m	5.23 m

both robustness and effectiveness, particularly in complex environments where the LOS path is obscured and in situations involving clutter and missed detections of MPC measurements.

REFERENCES

- [1] M. Z. Win, Y. Shen, and W. Dai, "A theoretical foundation of network localization and navigation," *Proc. IEEE*, vol. 106, no. 7, pp. 1136–1165, Jul. 2018.
- [2] H. Zhao, N. Zhang, and Y. Shen, "Beamspace direct localization for large-scale antenna array systems," *IEEE Trans. Signal Process.*, vol. 68, pp. 3529–3544, May 2020.
- [3] T. Deißler and J. Thielecke, "UWB SLAM with Rao-Blackwellized Monte Carlo data association," in *Proc. Int. Conf. on Indoor Positioning and Navigation*, Sep. 2010, pp. 1–5.
- [4] C. Gentner, T. Jost, W. Wang, S. Zhang, A. Dammann, and U. C. Fiebig, "Multipath assisted positioning with simultaneous localization and mapping," *IEEE Trans. Wireless Commun.*, vol. 15, no. 9, pp. 6104–6117, Sep. 2016.
- [5] H. Kim, K. Granström, L. Gao, G. Battistelli, S. Kim, and H. Wymeersch, "5G mmWave cooperative positioning and mapping using multi-model PHD filter and map fusion," *IEEE Trans. Wireless Commun.*, vol. 19, no. 6, pp. 3782–3795, Jun. 2020.
- [6] T. Wang, J. Liu, and Y. Shen, "A robust single-anchor localization method with multipath assistance in NLOS environments," in *Proc. IEEE Global Commun. Conf.*, Madrid, Spain, Dec. 2021, pp. 1–6.
- [7] H. Kim, H. Chen, M. F. Keskin, Y. Ge, K. Keykhosravi, G. C. Alexandropoulos, S. Kim, and H. Wymeersch, "RIS-enabled and access-point-free simultaneous radio localization and mapping," *IEEE Trans. Wireless Commun.*, Aug. 2023.
- [8] Z. Yang, H. Zhang, H. Zhang, B. Di, M. Dong, L. Yang, and L. Song, "MetaSLAM: Wireless simultaneous localization and mapping using reconfigurable intelligent surfaces," *IEEE Trans. Wireless Commun.*, vol. 22, no. 4, pp. 2606–2620, Apr. 2022.
- [9] J. Mullane, B.-N. Vo, M. D. Adams, and B.-T. Vo, "A random-finite-set approach to Bayesian SLAM," *IEEE Trans. Robot.*, vol. 27, no. 2, pp. 268–282, Apr. 2011.
- [10] K. Y. Leung, F. Inostroza, and M. Adams, "Multifeature-based importance weighting for the PHD SLAM filter," *IEEE Trans. Aerosp. Electron. Syst.*, vol. 52, no. 6, pp. 2697–2714, Dec. 2016.
- [11] B. Amjad, Q. Z. Ahmed, P. I. Lazaridis, M. Hafeez, F. A. Khan, and Z. D. Zaharis, "Radio SLAM: A review on radio-based simultaneous localization and mapping," *IEEE Access*, vol. 11, pp. 9260–9278, Jan. 2023.
- [12] R. Mahler, *Statistical multisource-multitarget information fusion*. Artech, 2007.
- [13] H. Zhao, M. Huang, and Y. Shen, "High-accuracy localization in multipath environments via spatio-temporal feature tensorization," *IEEE Trans. Wireless Commun.*, vol. 21, no. 12, pp. 10 576–10 591, Dec. 2022.
- [14] K. Murphy and S. Russell, "Rao-Blackwellized particle filtering for dynamic Bayesian networks," in *Sequential Monte Carlo methods in practice*. Springer, 2001, pp. 499–515.
- [15] M. S. Arulampalam, S. Maskell, N. Gordon, and T. Clapp, "A tutorial on particle filters for online nonlinear/non-Gaussian Bayesian tracking," *IEEE Trans. Signal Process.*, vol. 50, no. 2, pp. 174–188, Feb. 2002.
- [16] J. Houssineau and D. Laneuville, "PHD filter with diffuse spatial prior on the birth process with applications to GM-PHD filter," in *Int. Conf. Inf. Fusion*, Edinburgh, UK, Jul. 2010, pp. 1–8.
- [17] B.-n. Vo, M. Mallick, Y. Bar-Shalom, S. Coraluppi, R. Osborne, R. Mahler, and B.-t. Vo, "Multitarget tracking," *Wiley encyclopedia of electrical and electronics engineering*, no. 2015, 2015.